Lateral Diffusion Coefficients in Membranes Measured by Resonance Energy Transfer and a New Algorithm for Diffusion in Two Dimensions

Jósef Kuśba,* Li Li,† Ignacy Gryczynski,† Grzegorz Piszczek,† Michael Johnson,† and Joseph R. Lakowicz†
*Technical University of Gdańsk, Faculty of Applied Physics and Mathematics, Gdansk, Poland, and †University of Maryland School of Medicine, Center for Fluorescence Spectroscopy, Department of Biochemistry and Molecular Biology, Baltimore, Maryland 21201 USA

ABSTRACT We describe measurements of lateral diffusion in membranes using resonance energy transfer. The donor was a rhenium (Re) metal-ligand complex lipid, which displays a donor decay time near 3 μs. The long donor lifetime resulted in an ability to measure lateral diffusion coefficient below 10^{-8} cm^2/s. The donor decay data were analyzed using a new numerical algorithm for calculation of resonance energy transfer for donors and acceptors randomly distributed in two dimensions. An analytical solution to the diffusion equation in two dimensions is not known, so the equation was solved by the relaxation method in Laplace space. This algorithm allows the donor decay in the absence of energy transfer to be multiexponential. The simulations show that mutual lateral diffusion coefficients of the donor and acceptor on the order of 10^{-8} cm^2/s are readily recovered from the frequency-domain data with donor decay times on the microsecond timescale. Importantly, the lateral diffusion coefficients and acceptor concentrations can be recovered independently despite correlation between these parameters. This algorithm was tested and verified using the donor decays of a long lifetime rhenium lipid donor and a Texas red-lipid acceptor. Lateral diffusion coefficients ranged from 4.4×10^{-9} cm^2/s in 1,2-dimyristoyl-*sn*-glycero-3-[phospho-*rac*-(1-glycerol)] (DMPG) at 10°C to 1.7×10^{-7} cm^2/s in 1,2-dioleoyl-*sn*-glycero-3-phosphocholine (DOPC) at 35°C. These results demonstrated the possibility of direct measurements of lateral diffusion coefficients using microsecond decay time luminophores.

INTRODUCTION

Fluorescence spectroscopy has been widely used to measure the dynamic properties of cell membranes (Stubbs et al., 1992). Typically, the anisotropy decays of nanosecond decay time fluorophores are used to study the order and dynamics of the acyl side chain regions. Hence the anisotropy decays of nanosecond decay time membrane probes reveals membrane dynamics over distances of 2 to 10 Å. However, such studies provide no information on the lateral motions of lipids and proteins in biological membranes (Tocanne et al., 1994; Zhang et al., 1993; Walther et al., 1996; Edidin et al., 1994; Simson et al., 1995). Fluorescence recovery after photobleaching (FRAP) is presently the most commonly used method to measure lateral diffusion (Perisamy and Verkman, 1998; Lippincott-Schwartz et al., 1999; Valez and Axelrod, 1988). When using FRAP one measures the rates at which fluorophores repopulate a region of the membranes, which was photobleached by an intense laser light pulse. Hence FRAP measures lateral motions of lipids on proteins over large macroscopic distances ranging from 5000 to 30,000 Å. Such studies have shown that lipids or proteins do diffuse in membranes and that the rates of diffusion depend on the membrane lipid composition and the presence of membrane-bound proteins. Additionally, such measurements have revealed the presence of mobile and immobile fractions, the latter probably being proteins whose motions are restricted by the cytoskeleton matrix.

An alternative approach is to use resonance energy transfer (RET) to study the membranes (Fung and Streyer, 1978; Wolber and Hudson, 1979; Dewey and Hammes, 1986; Hauser et al., 1976; Estep and Thompson, 1979), which can be expected to provide information over distances comparable with the Forster distance (R_0), which are typically in the range of 25 to 60 Å. Such studies provide information on the spatial distribution and/or distance between donor (D) and acceptors (A). However, it is difficult to use RET to measure lateral diffusion coefficients. This is because there is little diffusive motion during decay times of the excited state, which are typically near 10 ns. The available expression for RET in two dimensions assumes a static distribution of donors and acceptors (Fung and Streyer, 1978; Wolber and Hudson, 1979; Dewey and Hammes, 1986; Hauser et al., 1976). To the best of our knowledge analytical expressions for RET in two dimensions with diffusion have not been reported.

In the present report we describe the use of RET to perform direct measurement of lateral diffusion in membranes. Such measurements are possible using luminescent metal-ligand complexes with microsecond decay times, many of which have been developed in this laboratory over the past several years (Terpetschnig et al., 1995, 1997; Szmacinski et al., 1996; Castellano et al., 1998; Guo et al., 1997). Because of the long decay times one can predict the lipids will undergo significant lateral motions during the excited state lifetime. It is well known that donor-to-accep-

Submitted June 5, 2000, and accepted for publication October 25, 2001.

Address reprint requests to Joseph R. Lakowicz, Univ. of Maryland School of Medicine, Center for Fluorescence Spectroscopy, Dept. of Biochemistry and Molecular Biology, 725 West Lombard St., Baltimore, MD 21201. Tel.: 410-706-7978; Fax: 410-706-8408; E-mail: jf@cfs.umbi.umd.edu.

Li Li's present address is National Institutes of Standards and Technology, Gaithersburg, Maryland.

M. Johnson's present address is Dr. Michael L. Johnson, Dept. of Pharmacology, University of Virginia, Charlottesville, VA 22908.

0006-3495/02/03/1358/15 $2.00

tor motions in three dimensions during the donor decay time result in an increased efficiency of energy transfer (Steinberg and Katchalski, 1968; Stryer et al., 1982; Thomas et al. 1978). The availability of metal-ligand complex (MLC)-labeled lipids with microsecond decay times thus suggests the possibility of measuring lateral diffusion coefficients in membranes for the time-resolved resonance energy transfer (RET) data. However, an analytical solution for the diffusion equations in two dimensions is not known. Hence, we developed a numerical algorithm that predicts the intensity decays of the donors in the presence of acceptors randomly distributed in two dimensions with mutual donor-to-acceptor diffusion. We show by simulations and experimental data that lateral diffusion coefficients can be readily recovered from the intensity decay of long-lived donors. These results demonstrate the possibility of measuring membrane dynamics on the heretofor inaccessible microsecond timescale over distances ranging from 20 to 100 Å.

THEORY

We now describe our method for simulations and analysis the time-resolved donor decays in the presence of two-dimensional diffusion of the donors and acceptors. Information about the static distribution and mutual donor-to-acceptor diffusion coefficient D is contained in the intensity decay of the donor. We assume that the donor emission can be observed without contributions from autofluorescence of the sample or from the fluorescent acceptor. We found that the intensity decay of the MLC donor in membranes was more complex than a single exponential even in the absence of acceptors. Hence, it was necessary to use expressions that account for a multiexponential decay law in the absence of energy transfer. The donor decays, in the absence of acceptors, were analyzed using the multiexponential model

$$I_D(t) = I_D^0 \sum_i \alpha_{Di} \exp(-t/\tau_{Di}), \tag{1}$$

in which I_D^0 is the intensity of the donor emission at time $t = 0$, and α_{Di} are the relative amplitudes (at $t = 0$) of the components characterized by the decay times τ_{Di} in the absence of acceptors. The factors α_{Di} are normalized so that $\sum_i \alpha_{Di} = 1$. Eq. 1 may be rewritten in the form

$$I_D(t) = \sum_i I_{Di}(t) \tag{2}$$

in which

$$I_{Di}(t) = I_D^0 \alpha_{Di} \exp(-t/\tau_{Di}) \tag{3}$$

are the intensity decays of the components with each decay time.

Because the decay of the donor is multi exponential even in the absence of acceptor, it is necessary to consider how energy transfer affects each component in the decay. We assume that the components behave as if they each have the same Förster distance (R_0) for transfer. Thus for the ith component of molecules containing a donor and an acceptor separated by a distance r, the transfer rate is described by

$$k_{DAi}(r) = \frac{1}{\tau_{Di}} \left(\frac{R_0}{r}\right)^6 \tag{4}$$

This assumption is frequently used when using RET to measure distance distributions and has not been found to introduce any difficulties (Cheung, 1991). Using this assumption, the donor decay in the presence of acceptors (Eq. 3) can be expressed as

$$I_{DAi}(t) = I_D^0 \alpha_i \exp[-t/\tau_{Di} - C_A^0 W_i(t)] \tag{5}$$

in which C_A^0 is the concentration of acceptor and $W_i(t)$ is given by

$$W_i(t) = \int_0^t k_i(t')dt'. \tag{6}$$

We assume here that energy transfer and/or diffusion modify only the $t > 0$ part of the donor fluorescence decay curve and does not change the time-zero characteristics of the decay, i.e., I_D^0 and α_i. The form of Eq. 4 does not depend on the dimensionality on the system. In contrast, the form of the second order donor-acceptor transfer rates, $k_i(t)$ are dimensionality dependent. Within a two-dimensional model for energy transfer with diffusion, the transfer rates $k_i(t)$ may be calculated as

$$k_i(t) = 2\pi \int_{r_{min}}^{\infty} r k_{DAi}(r) y_i(r, t) dr \tag{7}$$

in which r_{min} denotes the distance of donor-acceptor closest approach and $y_i(r, t)$ satisfy the diffusion equation

$$\frac{\partial y_i(r, t)}{\partial t} = D\nabla^2 y_i(r, t) - k_{DAi}(r) y_i(r, t) \tag{8}$$

with parameter D being a sum of the diffusion coefficients of the donor and acceptor, respectively ($D = D_D + D_A$). Functions $y_i(r, t)$ have a meaning of ratios of the mean concentration $C_{Ai}(r, t)$ of acceptor molecules at the distance r from the excited donor of the ith type to the bulk concentration of the acceptor C_A^0. The initial condition of Eq. 8 is

$$y_i(r, t = 0) = 1, \tag{9}$$

which means the donors and acceptors are randomly distributed at $t = 0$. The inner and outer boundary conditions are

$$\left[\frac{\partial y_i(r, t)}{\partial r}\right]_{r=r_{min}} = 0 \tag{10}$$

$$y_i(r \to \infty, t) = 1. \tag{11}$$

in which r_{min} is the distance of closest approach for the donor and acceptor. Eq. 11 can be understood as a constant

acceptor concentration at long distances from the donor. Eq. 10 is known as the reflection or specular boundary conditions, which assure that donor-acceptor collisions at $r = r_{min}$ do not influence the RET process except as due to the dependence on distance according to Eqs. 4 and 8. That is, the RET process is the only deactivation channel due to the acceptor.

An analytical solution of Eq. 8 is not known, so the numerical methods were applied. To minimize the time of calculation of the fluorescence decays with Eq. 5 we used an algorithm described previously (Kusba and Lakowicz, 1994). This algorithm allowed for variable mesh sizes on the time axis and for exponential approximation of the decay in the particular time intervals. To evaluate quantities $W_i(t)$ in Eq. 5, we applied a method similar to that described in (Kusba, 1987). Each of the decays from Eq. 5 was evaluated for approximately $n = 50$ time points, t_{ik}, ($k = 1..n$), inhomogenously distributed on the time axis. The intensity decays were calculated in Laplace space and inverted using the Stedfest procedure (Lakowicz and Gryczynski, 1991). More detail concerning the fluorescence decay evaluation can be found in the Appendix.

The calculated donor intensity decays were used to predict the phase and modulation values (Stehfest, 1970). For a given set of parameter values, D, τ, R_0, and r_{min}, the donor decays $I_{Di}(t)$ obtained by the numerical procedure were used for calculation of the quantities

$$N_\omega = \frac{\sum_i \int_0^\infty I_{Di}(t)\sin(\omega t)dt}{\sum_i \int_0^\infty I_{Di}(t)dt} \quad (12)$$

and

$$D_\omega = \frac{\sum_i \int_0^\infty I_{Di}(t)\cos(\omega t)dt}{\sum_i \int_0^\infty I_{Di}(t)dt} \quad (13)$$

at given modulation frequency ω. The values of N_ω and D_ω are needed for calculation (c) of the phase angle (φ_ω) and modulation (m_ω) values, which are given by

$$\varphi_{c\omega} = \arctan(N_\omega/D_\omega) \quad (14)$$

$$m_{c\omega} = (N_\omega^2 + D_\omega^2)^{1/2}. \quad (15)$$

The calculated phase ($\varphi_{c\omega}$) and modulation ($m_{c\omega}$) values are compared with the experimental data to determine the diffusion (D) parameter by the method of nonlinear least squares (Johnson, 1983; Johnson and Frasier, 1985). The goodness-of-fit is characterized by

$$\chi_R^2 = \frac{1}{\nu}\sum_\omega \left(\frac{\varphi_\omega - \varphi_{c\omega}}{\delta\varphi}\right)^2 + \frac{1}{\nu}\sum_\omega \left(\frac{m_\omega - m_{c\omega}}{\delta m}\right)^2 \quad (16)$$

in which ν is a number of degrees of freedom, and $\delta\varphi = 0.4°$ and $\delta m = 0.01$ are the experimental uncertainties in the measured phase angles (φ_ω) and modulation (m_ω), respectively, assumed for both the simulated and measured values. In the case of global analysis the sum in Eq. 16 extends over both the modulation frequencies (ω) and over the multiple data sets used in analysis. Typically these data are donor decays measured with different acceptor concentrations in the membranes or data with a single acceptor concentration but several temperatures.

The frequency-domain data were also analyzed in terms of multiexponential model Eq. 1. The fractional intensity of each component to the steady-state intensity is given by

$$f_{Di} = \frac{\alpha_{Di}\tau_{Di}}{\sum_j \alpha_{Dj}\tau_{Dj}}. \quad (17)$$

The mean lifetime is given by

$$\overline{\tau_D} = \sum_i f_{Di}\tau_{Di} \quad (18)$$

The confidence intervals on a parameter were determined from the dependence of χ_R^2 on this parameter when it was held constant at a value different from the optimal value. The other parameters were then allowed to vary to minimize χ_R^2 with the constant parameter held at its nonoptimal value, yielding χ_R^2 (par). This procedure yields the χ_R^2 surface on the contour plot for the parameter with the minimum value χ_R^2 (min) at the optimal parameter value. The contour plots are usually presented as the ratio

$$\chi_{RN}^2 = \frac{\chi_R^2\ (\text{par})}{\chi_R^2\ (\text{min})} \quad (19)$$

The ranges of parameter values consistent with the data were taken as the intersection of the χ_R^2 surface with the F_χ value for a given probability P, which we took as $P = 0.32$,

$$F_\chi = \frac{\chi_R^2\ (\text{par})}{\chi_R^2\ (\text{min})} = 1 + \frac{p}{\nu}F(p, \nu, P) \quad (20)$$

In this expression, $F(p, \nu, P)$ is the F-statistic with p parameters and ν degrees of freedom with a probability of P. In our experiments a single frequency domain data file contains about 40 measurements, 20 phase angles, and 20 modulation values. A global analysis is typically performed with five data files or 200 measurements. For 40 degrees of freedom and one variable parameters this value is $F_\chi \simeq 1.03$. For 200 degrees of freedom or five variable parameters $F_\chi \simeq 1.01$.

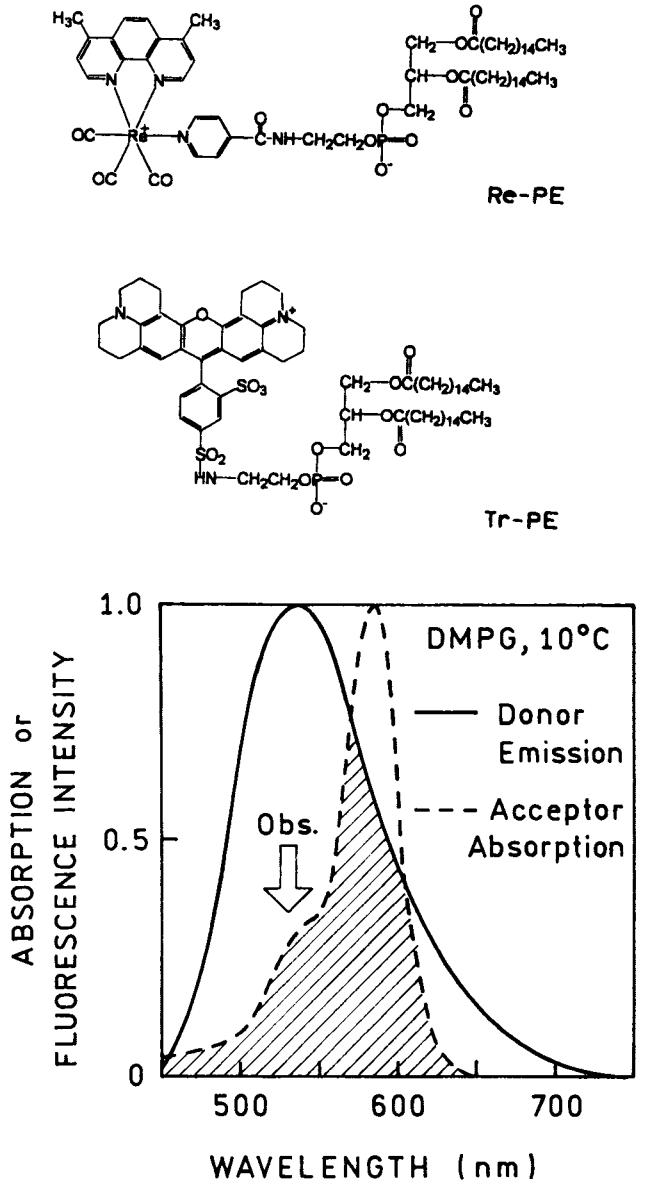

FIGURE 1 Molecular structure of the energy donor (Re-PE) and acceptor (Tr-PE). The lower panel shows the donor emission and acceptor absorption spectra. The shaded area in the overlap intergral corresponds to a R_0 value near 35 Å.

MATERIALS AND METHODS

The syntheses of [Re(4,7-Me_2phen)$(CO)_3$(4-COOHPy)](PF_6), where 4,7-Me_2phen is 4,7-dimethyl-1,10-phenanthroline and 4-COOHPy is isonicotinic acid, and its phospholipid analogue (Re-PE) serving as the energy donor were described in the previous reports (Li et al., 1999a, b). The energy acceptor, *N*-(Texas Red sulfonyl)-1,2-dihexadecanoyl-*sn*-glycero-3-phosphoethanolamine (Tr-PE), was obtained from Molecular Probes (Eugene, OR) and used as received. These chemical structures are shown in Fig. 1. The spectral properties of the donor and acceptor resulted in R_0 values near 35 Å, depending on the temperature. Under our experimental conditions the Förster distances (R_0) from Re-PE to Tr-PE energy transfer ranged from 28 to 37 Å. 1,2-dioleoyl-*sn*-glycero-3-phosphocholine (DOPC) and cholesterol were from Sigma Chemical Co (St. Louis, MO) and 1,2-dimyristoyl-*sn*-glycero-3-[phospho-*rac*-(1-glycerol)] (DMPG) was obtained from Avanti Polar Lipids (Alabaster, AL). All solvents and reagents were obtained from Aldrich and used without further purification. Water was deionized with a Milli-Q purification system.

Preparation of model membranes

Lipid vesicles were prepared by the usual procedure of mixing and sonication. Appropriate amounts of the donor and acceptor phospholipids, DMPG, DOPC, and/or cholesterol in $CHCl_3$ were taken from stock solutions, and the solvent was removed by a stream of argon. The molar ratio of Re-PE to Tr-PE was kept constant at 4.5:1 whereas the amount of unlabeled phospholipid was varied to obtain molar ratios of Tr-PE to DOPC ranging from 0 to 0.02. Vesicles were prepared by sonication under an atmosphere of argon in 0.1 M sodium phosphate buffer, pH 7.2, at final lipid concentrations ranging from 0.5 to 7.0 mg/ml. Using this preparation procedure, the vesicle diameter is between 200 and 250 Å as determined through anisotropy measurements using the long lifetime ruthenium complex lipid (Li et al., 1997). For all simulations and analyses we assumed the minimum donor-to-acceptor distance was $r_m = 7$ or 8 Å as indicated in the text. The area occupied per lipid molecules was assumed to be 74 $Å^2$/lipid molecules for DOPC at all temperatures, 48, 55, and 62 Å/lipid molecule for DMPG at 10.23 and 35 ÅC, respectively, and 55 Å/molecule for cholesterol at all temperatures (Marra, 1986). The Förster distance (R_0) was calculated using the known equations and the uncorrected emission spectra of the Re-PE labeled vesicles. Quantum yields of Re-PE were measured relative to 3-aminofluoranthene in dimethyl sulfoxide with an assumed quantum yield of 0.32 (Gryczynski et al., 1997). For calculating the overlap intergral we used the absorption spectrum of Tr-PE with a maximum extinction coefficient of 109,000 M^{-1} cm^{-1} at 583 nm.

Instrumentation

Absorption and emission spectra were recorded on a HP 8453 diode array spectrophotometer and a SLM AB2 fluorimeter under magic angle polarization conditions, respectively. The frequency-domain fluorimeter (ISS, Koala) used 325-nm excitation from a HeCd laser (Liconix, 20 mW). This laser was passed through a Pockels cell operated from an ISS low frequency amplifier (K2.LF), which provided modulated light from 3 kHz to 2.5 MHz. Two PTS frequency synthesizers (PTS-500) were used to modulate the Pockels cell and detection system. For fluorescence intensity measurements, a 500-nm cutoff filter (500FH90-50S) and two short-wavelength pass filters (550FL07-50S) from Andover (Salem, NH) were used to isolate the donor emission from that of the acceptor.

RESULTS

Effect of two-dimensional diffusion on the transfer efficiency

Prior to considering the intensity decays of the donors it is informative to examine the effect of two-dimensional diffusion on the overall transfer efficiency. The transfer efficiency (E) was calculated from the integral of the time-

dependent donor decay in the absence ($I_D(t)$) and presence ($I_{DA}(t)$) of acceptors using

$$E = 1 - \frac{\int_D^\infty I_{DA}(t)dt}{\int_D^\infty I_D(t)dt} \quad (21)$$

in which the superscript A indicates the presence of acceptor.

Fig. 2 shows the transfer efficiencies for various assumed donor decay times and mutual diffusive coefficients. The acceptor density was assumed to be 5×10^{-3} acceptors/lipid. For typical donor decay times near 10 ns even rapid lateral diffusion at 10^{-6} cm^2/s will not effect the transfer efficiency. As the donor decay time increases the transfer efficiency increases. For very long decay times and/or rapid lateral diffusion the transfer efficiency approaches a limiting value of 91.4% (Fig. 2, – – –). This is the rapid diffusion limit at which the transfer efficiency is determined by the distance of closest approach between the donor and acceptor. For spherical donors and acceptors in two dimensions the diffusion limited value of the rate of energy transfer k_T is given by

$$k_T = \frac{1}{\tau_D}\int_{r_{min}}^\infty \left(\frac{r}{R_0}\right)^6 \alpha_A 2\pi r dr = \frac{\pi\sigma_A R_0^6}{2r_{min}^4} \quad (22)$$

in which $\sigma_A = 6.7 \times 10^{-5}$ molecules/Å^2 is the density of acceptors, $r_{min} = 7$ Å is the distance of closest approach, $R_0 = 25$ Å, and $\tau_D = 3$ μs is the donor decay time (Thomas and Stryer, 1982; Stryer et al., 1982; Lakowicz, 1999). Using these values one can calculate the diffusion limited value of k_T to be 3.55×10^6 s^{-1} = $10.65/\tau_D$. The diffusion limited transfer rate is ~10-fold larger than the donor-donor decay time. This value of k_T can be used to calculate the transfer efficiency of 91.4% using

$$E = \frac{k_T}{k_T + \tau_D^{-1}}. \quad (23)$$

Additional information is available if the donor decay times are intermediate between the static and rapid diffusion limit, where the transfer efficiency depends on the mutual donor-to-acceptor diffusion coefficient (Fig. 2). In particular, for decay times from 1 to 100 μs, lateral diffusion coefficients from 10^{-9} to 10^{-6} cm^2/s result in increased transfer efficiency. These results suggest that the time-dependent donor decays can be used to measure the rate of donor-to-acceptor diffusion in membranes.

Simulated time-dependent donor decay with RET and two-dimensional diffusion

We used our numerical algorithm for RET in membranes to simulate the frequency-domain intensity decays. The frequency responses were simulated using assumed values of R_0, lipid area, and acceptor density. Simulated data for unquenched donor decay times (τ_D) of 3 and 30 μs are shown in Fig. 3. The solid and dashed lines show the donor decays in the presence and absence of diffusion, respectively. These frequency responses show that faster diffusion shifts the response to higher frequencies and shorter mean donor decay times. For the same diffusion coefficients longer donor decay times result in larger shifts, as expected with the additional time for D-to-A diffusion. Analytical expressions are available for RET in two dimensions without diffusion (Wolber and Hudson, 1979; Dewey and Hammes, 1986; Hauser et al., 1976; Estep and Thompson, 1979). We confirmed that the frequency responses calculated using our algorithm without diffusion (– – –) were equivalent to the known analytical expressions.

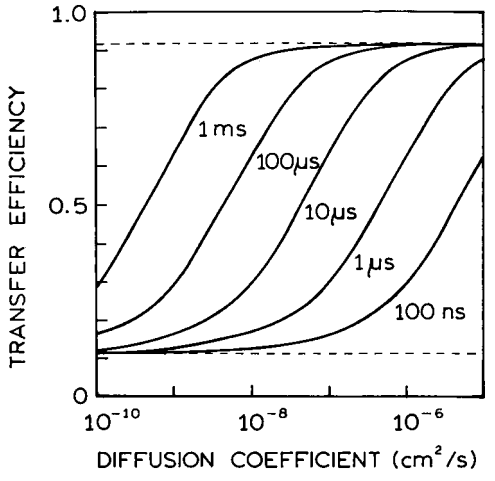

FIGURE 2 Effect of the lateral diffusion coefficient and the donor decay time on the steady-state RET transfer efficiency. For these simulations we assumed $r_{min} = 7$ Å, $R_0 = 25$ Å, 75 Å^2 per lipid molecule and 5×10^{-3} acceptor per lipid molecule.

In an experimental analysis we wish to calculate the diffusion coefficient from the time-resolved data. The ability to recover D from the frequency-domain data is not obvious because increased diffusion coefficients and increased acceptor densities both result in higher amounts of energy transfer. Stated alternatively, one can expect the diffusion coefficient and acceptor density to be correlated parameters (Johnson, 1983). Hence we analyzed the frequency-domain data simulated with various acceptor densities and a mutual diffusion coefficient of 10^{-7} cm^2/s (Table 1). One notices that the correct values of both D and the A density were recovered over a range of acceptor densities. The uncertainty in the recovered parameter is reasonably small. These values were obtained with both the diffusion coefficients and acceptor concentrations as variable parameters. Because higher diffusion coefficients and higher acceptor concentrations both result in an increase in the transfer efficiency these parameters are expected to be

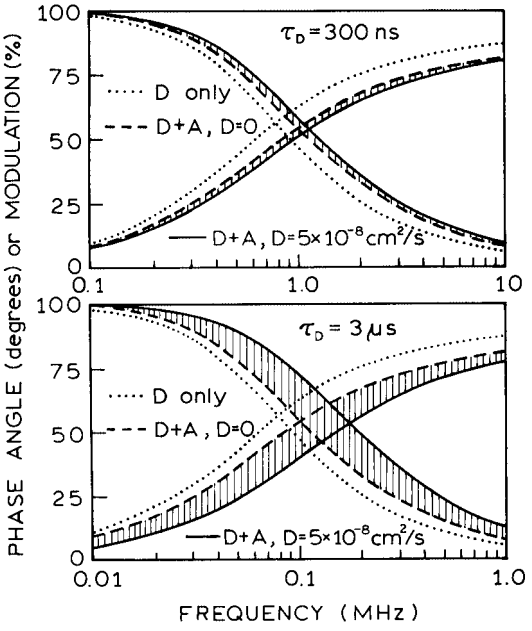

FIGURE 3 Simulated frequency-domain intensity decays for donors and acceptors randomly distributed in two dimensions. For the simulation, $R_0 = 25$ Å $r_{min} = 7$ Å, 75 Å^2/lipid molecule, and 5×10^{-3} acceptors/lipid molecules. For $D = 5 \times 10^{-8}$ cm^2/s the solid lines show the simulated phase and modulation values. The dashed lines show the expected donor decays without lateral diffusion, and the dotted lines show the donor decays in the absence of acceptors. The shaded area shows the contribution of lateral diffusion to increasing the rate of energy transfer.

TABLE 1 Energy transfer and diffusion analysis* of simulated data

Acceptor/lipid × 10^3		$D \times 10^7$	
Simulated	Recovered	(cm^2/s)	χ^2_R
2.0	2.02	0.93	1.04
	(1.72–2.39)	(0.67–1.20)†	
	7.03	⟨0⟩	8.13
4.0	4.11	0.94	0.90
	(3.67–4.61)	(0.74–1.14)	
	13.3	⟨0⟩	22.3
8.0	8.23	0.95	1.49
	(7.29–8.90)	(0.82–1.19)	
	25.1	⟨0⟩	41.9
12.0	11.6	1.07	1.09
	(11.1–12.1)	(1.00–1.14)	
	35.9	⟨0⟩	64.0
Global			
2.0	1.94	0.998	1.08
	(1.78–2.09)	(0.89–1.15)	
4.0	3.97	–	–
	(3.67–4.25)		
8.0	8.04	–	–
	(7.43–8.59)		
12.0	12.1	–	–
	(11.1–12.7)		
2.0	7.11	⟨0⟩	34.1
4.0	13.3		
8.0	25.1		
12.0	35.9		

Results of fit to diffusion coefficient and acceptor concentrations.
*For simulations we used $\tau_D = 2500$ ns, $R_0 = 35$ Å, $D = 10^{-7}$ cm^2/s, $\delta\varphi = 0.4°$, and $\delta m = 0.01$. The area occupied by an individual lipid and the minimum donor-acceptor distance were assumed equal to 74 Å^2 and 8.6 Å, respectively.
†The numbers in parentheses represent the confidence intervals obtained from the least-squares analysis with consideration of correlation between the diffusion coefficient and the acceptor density.

correlated. More specifically, an increase in the diffusion coefficient can be compensated for by a decrease in the acceptor concentration and vice versa. Correlation between parameters results in wider confidence intervals than for uncorrelated parameters (Johnson, 1983; Johnson and Frasier, 1985). Even with consideration of correlation the confidence intervals are small, ~10% of the assumed values. The ability to recover both the diffusion coefficients and the acceptor density can be understood as the effects of diffusion on the form of the intensity decay. Energy transfer to a static distribution of acceptors, in 1, 2 or 3 dimensions, results in nonexponential decays (Thomas and Stryer, 1982). As the diffusion coefficient increases the donor decays become shorter but more like a single exponential (Lakowicz, 1999). It is this dependence on the form of the intensity decay on the diffusion coefficient, which allows recovery of both D and A density from the time-resolved data.

We used simulations to estimate the lower limit of the diffusion coefficient, which we expect to be detectable with a 3-μs decay time donor (Fig. 4). The shaded areas indicate the contribution of diffusion to increasing the donor decay rate. These simulations show that diffusion coefficient as low as 5×10^{-9} cm^2/s still visually alter the donor decays. We performed additional simulations to more quantitatively predict the lower limit of the diffusion coefficient detectable with a 3-μs decay time donor. This was accomplished by simulating data for assumed diffusion coefficients and acceptor concentrations. The simulated data were then analyzed to recover the χ^2_R values with the diffusion coefficient and acceptor density as variable parameters (χ^2_R) or with the diffusion coefficient set to zero $\chi^2_R(D = 0)$. This difference between these fits reflects the possibility of compensating for a higher diffusion coefficient with a lower acceptor concentration. In these analyses the acceptor concentrations were either held fixed at the assumed value (Fig. 5, top) or taken as a variable parameter (Fig. 5, bottom). When the acceptor concentration is fixed the relative elevation of the χ^2_R ratio indicates the overall contribution of acceptor presence and diffusion on the donor decay. In this case one sees that diffusion coefficients less than 10^{-9} cm^2/s are detectable (Fig. 5, top). If the acceptor concentration is a variable parameter the lowest detectable diffusion coefficient is again near 10^{-9} cm^2/s (Fig. 5, bottom). With the acceptor concentration as a variable parameter the increase in χ^2_R are

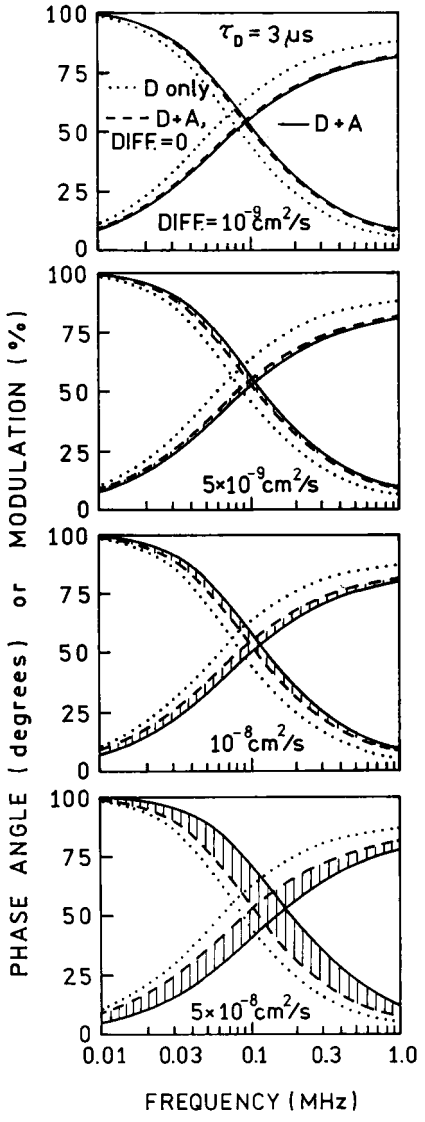

FIGURE 4 Simulated donor intensity decay for a donor decay time τ_0 = 3 μs and various lateral diffusion coefficients. For these simulations R_0 = 25 Å, r_{min} = 7 Å, 75 Å^2 per lipid molecule, and 5 × 10^{-3} acceptors per lipid molecule.

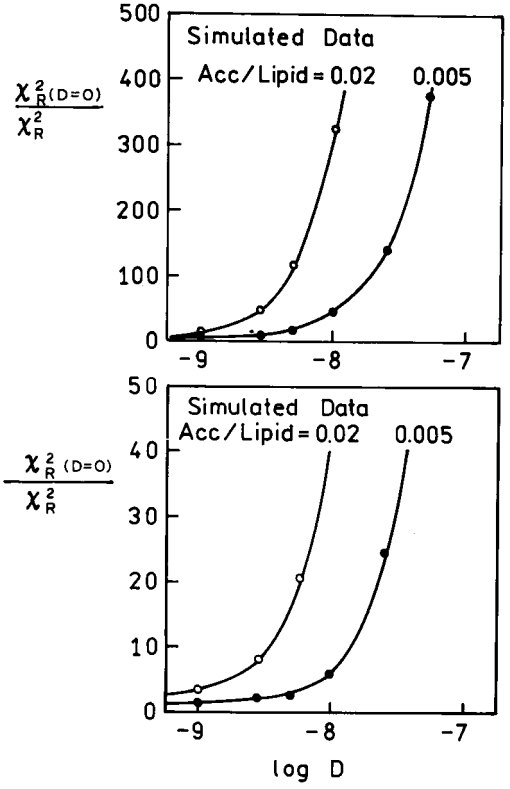

FIGURE 5 Relative χ^2_R values for data simulated with D-to-A diffusion and an acceptor-to-lipid ratio of 0.02. The simulated data were analyzed with and without D-to-A diffusion. The simulated data were analyzed with the acceptor concentration fixed at the known value (*top*) or as a floating parameter (*bottom*). The assumed values are τ_D = 3 μs, R_0 = 25 Å, r_{min} = 7 Å, and 75 Å^2 per lipid molecule. For D = 10^{-9} cm^2/s the ratio of χ^2_R (D = 0)/χ^2_R with the acceptor concentration fixed at 0.02 is 8.8 (*top*). With the acceptor concentration floating the ratio is 3.4.

~10-fold less than with a known acceptor concentration. Nonetheless, the relative χ^2_R values are significantly elevated, which reflect the effect of diffusion on changing the shape of the frequency response as well as its position on the frequency axis. In both cases somewhat lower diffusion coefficients are detectable at higher acceptor concentrations.

Experimental measurements of RET in membranes

Prior to measurement of RET in membranes we examined the intensity decays of Re-PE in lipid bilayers in the absence of acceptor (Fig. 6 and Table 2). The Re-PE intensity decays were found to be described by a double or triple exponential decay with mean decay times ranging from 2.2 to 0.5 μs. The longest mean decay times were observed in the absence of cholesterol at the lower temperature. These intensity decays in Table 2 were used as fixed values when analyzing the donor decays in the presence of the RET acceptors.

We next examined the donor decays in the presence of the Tr-PE acceptor. These measurements were performed in unsaturated DOPC vesicles (Fig. 7), saturated DMPG vesicles (Fig. 8) and in DMPG vesicles containing cholesterol (Fig. 9). In all cases the donor frequency responses were adequately fit to our model with the diffusion coefficient and the acceptor density as floating parameters (Table 3). The contributions of diffusion-enhanced RET to the donor decays can be seen by comparing the measured response with that calculated with D = 0 (- - -). In DOPC mutual donor-to-acceptor diffusion makes a substantial contribution towards increasing the donor decay rate at all temperatures from 10 to 35°C (Fig. 7). In the case of DMPG the effect of diffusion is minimal below its

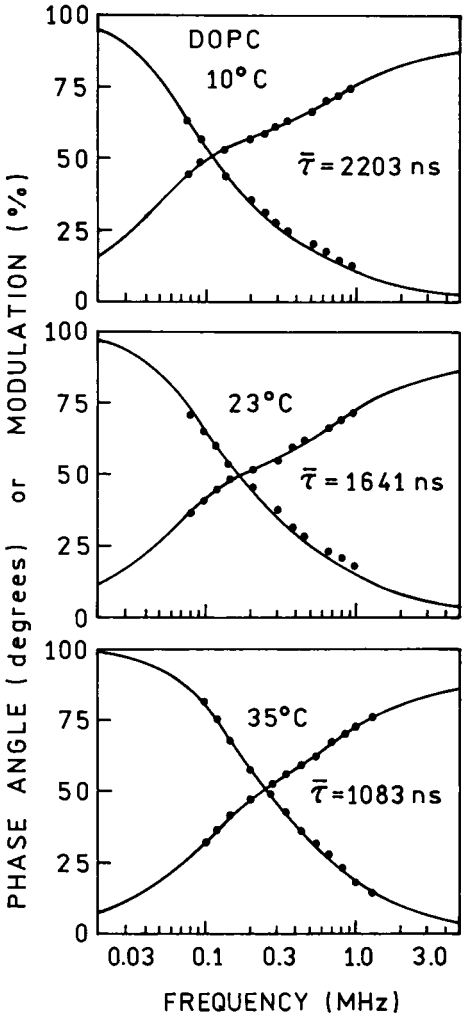

FIGURE 6 Intensity decay of Re-PS in DOPC in the absence of acceptor.

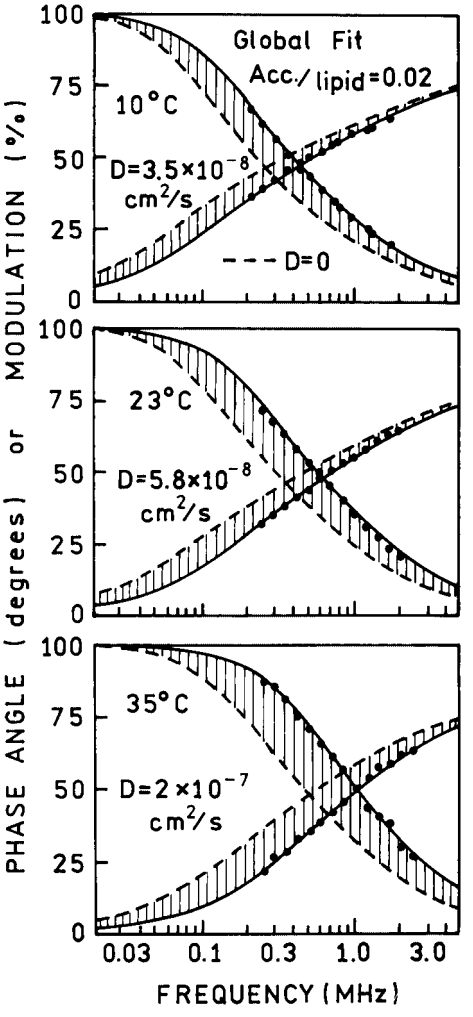

FIGURE 7 Re-PE donor decays in DOPC in the presence of a 0.02 mol fraction of Tr-PE acceptor. The solid line shows the best fit with the diffusion coefficient and acceptor density as variable parameters. The dash line shows the predictive response at the known acceptor density and the diffusion coefficient set equal to zero.

transition temperature of 23°C, and the effect of diffusion is evident at 35°C (Fig. 8). In the case of DMPG vesicles, which also contain cholesterol the contribution of diffusion is modest but visible from 10 to 35°C.

Fig. 10 summarizes the lateral diffusion coefficients obtained from the RET data. These diffusion coefficients were

TABLE 2 Multiexponential analysis of the Re-PE donor intensity decays in lipid vesicles

Lipid, Temp.	$\bar{\tau}_D$* (ns)	τ_1 (ns)	τ_2 (ns)	τ_3 (ns)	α_1	α_2	α_3	χ^2_R
DOPC, 10°C	2203.4	323.6	2504.3	–	0.552	0.448	–	2.5†
DOPC, 23°C	1640.9	301.6	1955.0	–	0.604	0.396	–	5.3
DOPC, 35°C	1082.8	295.0	1287.2	–	0.532	0.468	–	2.1
DMPG, 10°C	2350.7	179.6	1330.7	4243.9	0.263	0.619	0.118	2.2
DPMG, 20°C	848.1	80.4	750.4	1840.0	0.235	0.728	0.037	2.3
DMPG, 35°C	491.6	48.1	603.9	–	0.206	0.794	–	1.6
DPMG, Chol 10°C	1386.8	257.6	1681.6	–	0.631	0.369	–	2.1
DMPG, Chol 23°C	819.1	234.9	1071.8	–	0.664	0.336	–	2.2
DMPG, Chol 35°C	516.1	150.1	597.6	–	0.469	0.531	0	3.6

*$\bar{\tau} = \Sigma_i\, \alpha_{Di}\tau_{Di}^2/\Sigma_j\, \alpha_{Dj}\tau_{Dj} = \Sigma_i\, f_{Di}\tau_{Di}$.
†$\delta\varphi = 0.4°$ and $\delta m = 0.01$.

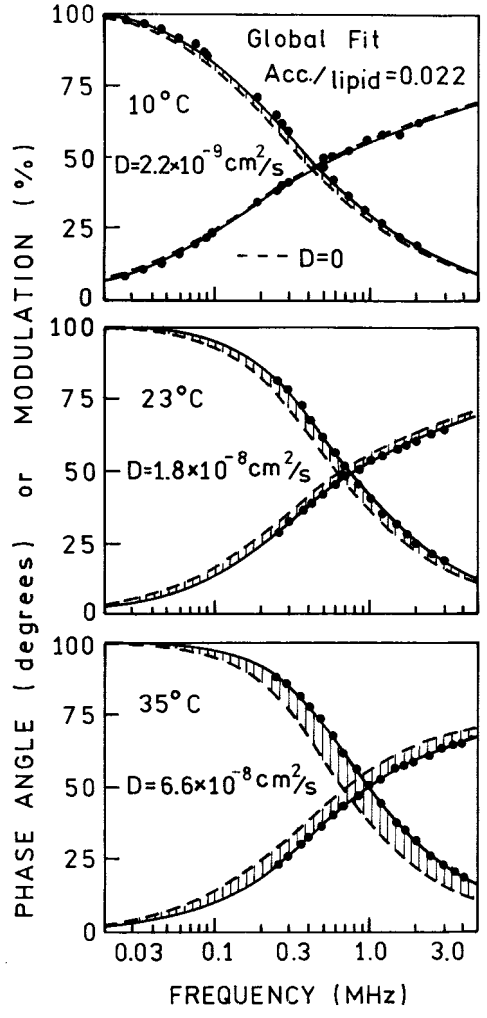

FIGURE 8 Re-PE donor decays in DMPG in the presence of a 0.02 mol fraction of Tr-PE acceptor. The DMPG/cholesterol ratio is 4:1. See Fig. 7.

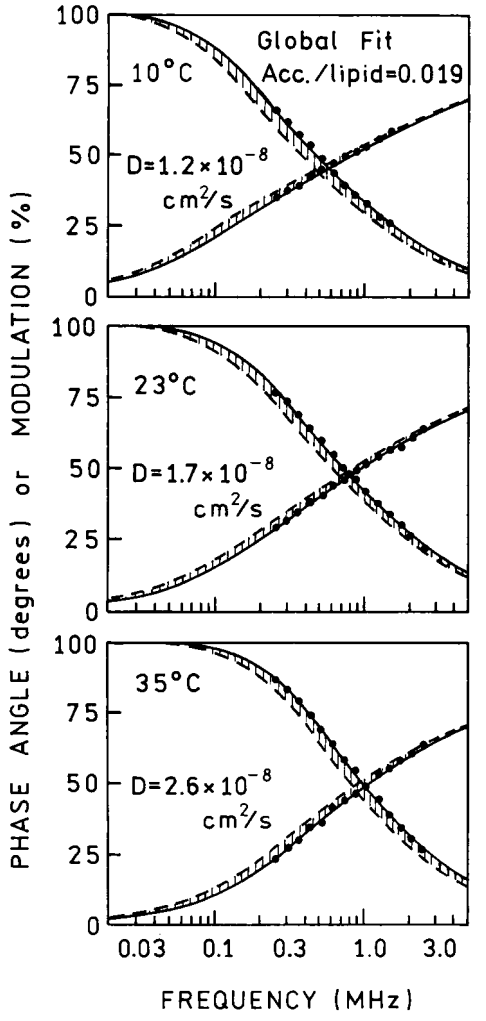

FIGURE 9 Re-PE donor decays in DMPG/cholesterol (mol/mol) in the presence of a 0.02 mol fraction of Tr-PE acceptor. See Fig. 7.

recovered from the global analysis at three temperatures with the single acceptor concentration in the membrane as a global parameter (Table 3). The largest diffusion coefficients were observed in DOPC bilayers, but the effect of temperature was modest (Fig. 10). Lower diffusion coefficients were observed in DMPG bilayers, but these values were strongly dependent on temperature. The presence of cholesterol in the DMPG bilayers resulted in an intermediate rate of diffusion and in a weaker dependence of the lateral diffusion coefficient on temperature.

We questioned the uncertainty in the recovered values of the diffusion coefficients. As has been discussed previously, there is no analytically correct method to calculate the uncertainty for parameters recovered from nonlinear least squares analysis (Johnson, 1983; Johnson and Frasier, 1985). However, these uncertainties can be obtained by examination of the χ^2_R surfaces or contour plots. To construct such a plot one repeats the least squares analysis with a chosen parameter value fixed at a value near to but not at the value yielding the minimum value of χ^2_R. The other parameters are allowed to vary to minimize χ^2_R. This new χ^2_R value represents that found for the fixed parameter value with adjustment of all the other parameters to improve the fit. Because the other parameters can vary this procedure accounts for correlation between the parameters. If the parameters are completely correlated, such as an product of two terms, then changes in one parameter can be completely compensated by a change in the second parameter.

The χ^2_R surfaces for RET in the DOPC and DMPG vesicles are shown in Figs. 11 and 12, respectively. For a single temperature the χ^2_R surfaces for both the diffusion coefficient and acceptor concentrations are well defined. This is an important result, which indicates the diffusion coefficients and acceptor concentrations are not completely correlated. Furthermore, the range of diffusion coefficients and acceptor concentrations consistent with the data are relatively small. For instance, for DOPC at 20°C these values range from 7.7×10^{-8} to 6.1×10^{-8} cm^2 and 0.0174 to 0.0192 acceptors per lipid.

TABLE 3 Analysis of the Re-PE donor decays in terms of the mutual D-to-A diffusion coefficient

Lipid, Temp.	R_0 (Å)	F/F_0*	Accept or/lipid	D (cm^2/s)	χ^2_R	χ^2_R ($D = 0$)	χ^2_R (three-dimensional model)‡
DOPC							
10°C	37.1	0.20	0.0204	3.1×10^{-8}	1.0†	33.6	1.3
23	35.3	0.22	0.0182	6.9×10^{-8}	1.4	66.2	2.6
35	32.9	0.19	0.0201	1.6×10^{-7}	2.3	105.4	2.7
Global							
10°C	37.1	0.20		3.5×10^{-8}			
23	35.3	0.21		5.8×10^{-8}			
35	32.9	0.15	0.0195	1.7×10^{-7}	1.6	116.6	3.2
DMPG							
10°C	36.7	0.15	0.0206	4.4×10^{-9}	2.6	7.5	8.3
23	31.1	0.23	0.0237	1.1×10^{-8}	1.3	5.1	6.4
35	29.1	0.24	0.0289	2.3×10^{-8}	1.4	6.0	4.3
Global							
10°C	36.7	0.14		2.2×10^{-9}			
23	31.1	0.24		1.8×10^{-8}			
35	29.1	0.26	0.0220	6.6×10^{-8}	4.0	45.1	15.3
DMPG/Chol							
10°C	33.6	0.26	0.0176	1.6×10^{-8}	1.0	11.2	1.3
22	30.9	0.30	0.0191	1.2×10^{-8}	1.2	6.5	
35	28.2	0.36	0.0177	3.2×10^{-8}	1.4	9.9	1.6
Global							
10°C	33.6	0.25		1.2×10^{-8}			
23	30.9	0.31		1.7×10^{-8}			
35	28.2	0.36	0.0186	2.6×10^{-8}	1.8	9.5	2.2

*These values of the relative donor fluorescence in the absence (F_0) and presence (F) of acceptors were calculated using the recovered values of D and the acceptor density.

†$\delta\varphi = 0.4°$ and $\delta m = 0.01$.

‡For these analyses the data were fit to a model for RET between donors and acceptors randomly distributed in three dimensions.

These results mean that the RET data can be used to recover both values. This possibility will become important in studies of isolated cell membranes or intact cells where it is not always possible to know the probe concentrations.

The confidence intervals for the diffusion coefficient and acceptor concentrations can be decreased by a global analysis. In these cases (Figs. 11 and 12) we used the acceptor concentration as a global parameter and allowed the diffusion coefficients to be different at each temperature. The χ^2_R surfaces (——) were calculated for changing just one of the three diffusion coefficients or the acceptor concentration. The confidence intervals are smaller than for a single data file mostly because of the lower χ^2_R ratio (● ● ●) needed for significance because of the larger number of data points. In these cases global analysis results in an approximate twofold decrease in the confidence interval. These ranges are shown in Fig. 10. It is interesting to notice that the largest confidence interval was found for DMPG 10°C. This can also be seen from the χ^2_R surface in Fig. 12. In this lipid the rate of diffusion below the phase transition temperature is slow, even on the microsecond timescale. The small contribution of diffusion to the donor decay results in a larger uncertainty in this slower diffusion coefficient.

It is informative to question whether the data are sensitive to the dimensionality of the system. More specifically, can the data distinguish between donors and acceptors distrib-

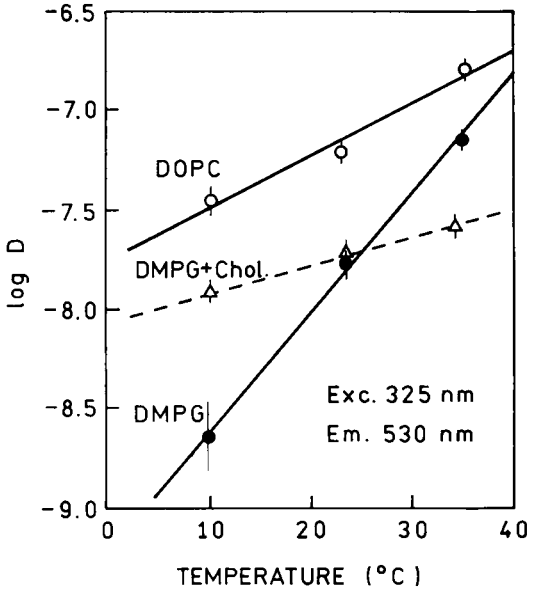

FIGURE 10 Temperature-dependent lateral diffusion coefficient in membranes as observed using the Re-PE and Tr-PE donor-acceptor pair. The diffusion coefficients are from the global analysis at three temperatures and one lipid concentration (Table 3). The error bars represent the confidence intervals obtained from the global analysis at one acceptor concentration and three temperatures (Figs. 11 and 12).

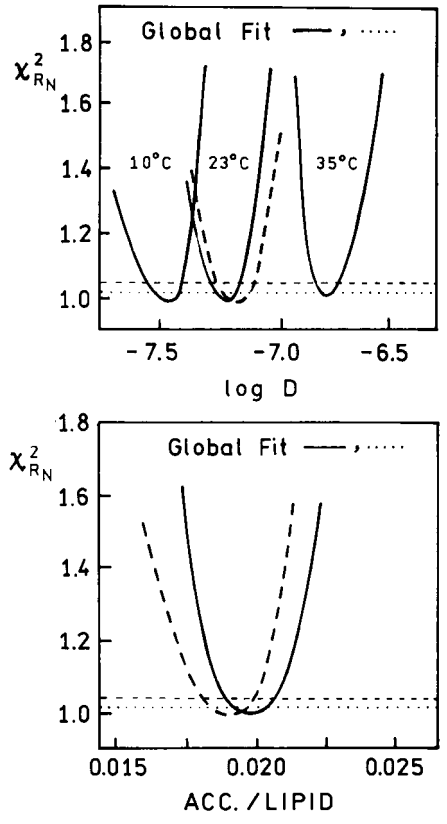

FIGURE 11 Resolution of the lateral diffusion coefficient and acceptor concentration in DOPC vesicles as seen for the χ^2_R surfaces. The values χ^2_R are the χ^2_R values normalized to the minimum χ^2_R value. The solid and darker dashed lines represent the global and nonglobal fits, respectively. The dotted and lighter dashed lines represents the upper value of the χ^2_R ratio consistent with the data.

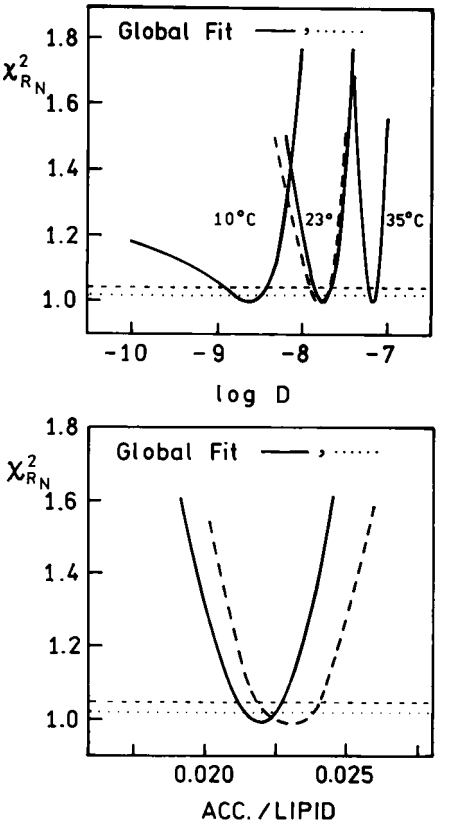

FIGURE 12 Resolution of the lateral diffusion coefficient and acceptor concentration in DMPG vesicles as seen for the χ^2_R surfaces. The values of χ^2_R are from the global analysis at three temperatures. The solid and darker dashed lines represent the global and nonglobal fits, respectively. The dotted and lighter dashed lines represents the upper value of the χ^2_R ratio consistent with the data.

uted randomly in two or three dimensions. The frequency-domain data were analyzed in terms of a model for diffusing donors and acceptors in three dimensions (Kusba et al., 2000). These analyses result in χ^2_R values, which are somewhat elevated over our two-dimensional model (Table 3). However, most of the χ^2_R values are reasonably low, and the fits may be regarded as adequate. However, despite these low χ^2_R values, the results of the analyses are unacceptable because the answers are not reasonable. These analyses result in acceptor concentrations of 12 to 80 mM and diffusion coefficients ranging from 10^{-7} to 10^{-15} cm^2/s. The acceptor concentrations are unacceptably large and much higher than the known bulk concentration of the acceptors.

And finally we questioned whether the frequency-domain donor decays, measured for multiple acceptor concentrations, would result in improved resolution of the diffusion coefficients. The donor decays from a range of acceptor concentrations in DOPG vesicles are shown in Fig. 13. The solid lines show the best fit when the acceptor concentrations are variable and there is a single global diffusion coefficient. Except for an acceptor density of 0.005, the data are well matched with a single diffusion coefficient. The χ^2_R surfaces shows little if any decrease in the confidence intervals. Hence, there seems to be little advantage to measuring the donor decay at multiple acceptor concentrations.

DISCUSSION

A variety of methods have been used to study lateral diffusion in membranes (Tocanne et al., 1994). The fluorescence methods include quenching, pyrene excimer formation, and RET. Collisional quenching requires close contact between the fluorophores and quencher. As a result most fluorophores in membranes except pyrene are not significantly quenched by reasonable quencher concentrations. Pyrene excimer formation is useful but limited to pyrene and closely related fluorophores, limited by the approximate 200-ns decay time of pyrene in membranes, by the existence

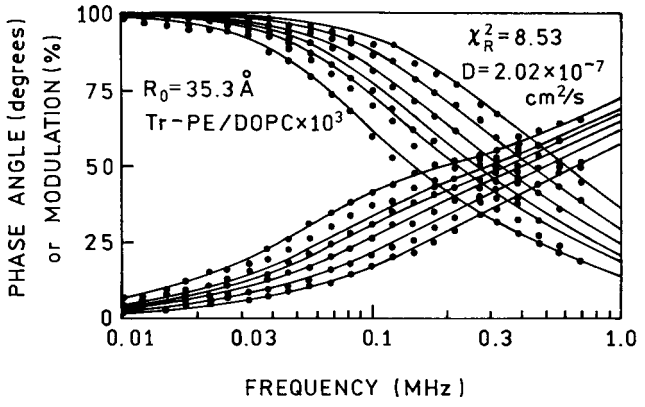

FIGURE 13 Frequency-domain intensity decay of Re-PE in DOPC with various concentrations of acceptor. The solid line shows the global analysis using a single diffusion coefficient. From left to right the acceptor densities were 0.025, 0.005, 0.01, 0.015, and 0.02 acceptors per lipid.

of preformed complexes, and by the possibility that the efficiency of excimer formation in different membrane environments. In contrast, RET seems to be preferred over quenching and excimer formation. RET is a through-space interaction that occurs over longer distances and is not affected by the local or intervening environment. Additionally, longer lifetimes and a wide range of spectral properties can be obtained from the extensive literature on metal-ligand complexes (Kalayanasundaram, 1992; Juris et al., 1988; Demas and DeGraff, 1997). Still longer decay times near 0.5 to 3.0 ms can be obtained with lanthanide chelates (Sabbatini and Guardigli, 1993; Li and Selvin, 1995; Martin and Richardson, 1979; Horrocks and Sudnick, 1981; Chen and Selvin, 2000). Given the availability of theory to predict two-dimensional RET with diffusion, we believe that RET with long decay time donors offers considerable promise for studying lateral transport in membranes.

It is reasonable to question whether long lifetime donors can be used in living cells. The use of cells raises two issues: uptake of the labeled lipid and detectability of the emission. Although not easy, cell membranes are frequently labeled with fluorescent fatty acids and lipids (Fulbright et al., 1997; Zucker, 2001; Tocanne et al., 1994; Struck and Pagano, 1980; Tanhuanpää and Somerharju, 1999). Because the metal-ligand complexes display good water solubility, it is probable that labeling with MLC-lipids can be accomplished. However, the MLC probes are less bright than typical organic fluorophores due to their lower extinction coefficient and lower quantum yields. The low extinction coefficients can be circumvented by the use of tandem fluorophores (Tyson and Castellano, 1999a,b; Zhou et al., 2000). These probes contain a high extinction coefficient absorber, which donates the energy to the MLC acceptor with high efficiency. Additionally, it is now known that the effective quantum yield of MLCs can be increased by RET to high quantum yield acceptors (Lakowicz et al., 2001; Maliwal et al., 2001). Hence it appears likely that RET from long lifetime donors can be used with living cells.

In the future one can imagine the use of microsecond and millisecond decay time donors to study slower or more complex motions in membranes. As examples, it is known that membranes form domains of solid and liquid phases (Thompson et al., 1995; Jorgensen et al., 1996; Gheber and Edidin, 1999; Matko and Edidin, 1997). Also, lateral diffusion of lipids is expected to depend on the presence of proteins, which slow lipid diffusion or prevent the motions of proteins (Marguet et al., 1999; Kenworthy and Edidin, 1998). Analysis of the motions in such systems will require further development of the theory and programs to extract the relevant molecular information from the intensity decays.

APPENDIX

At the beginning of calculation of the fluorescence decay $I_{Di}(t)$ according to the algorithm described in Kusba and Lakowicz (1994) one has to

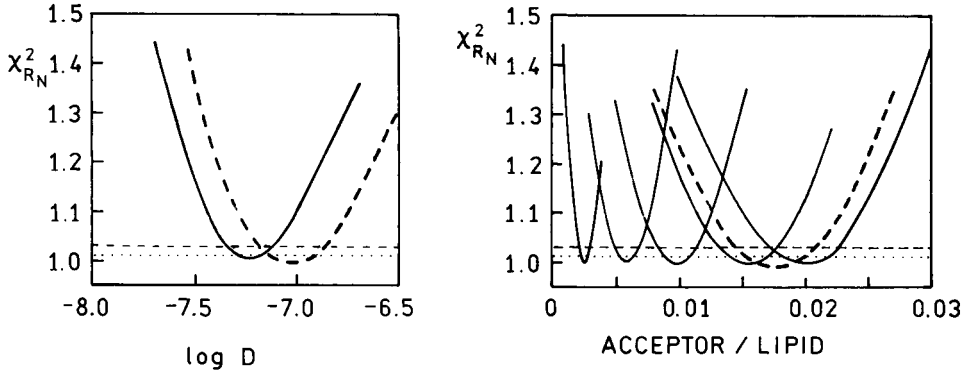

FIGURE 14 χ_R^2 surfaces for the lateral diffusion coefficient and acceptor concentrations in DOPC at 20°C. The bold solid lines and bold dashed lines represent the global fit with a single diffusion coefficient to the data at 5 or 1 acceptor density, respectively. The lighter dotted and dashed lines indicate the confidence intervals for the fits with 5 or 1 acceptor densities, respectively.

evaluate the length of the first step, Δt_{i1}, on the time axis. In our calculations Δt_{i1} was found from the relation

$$\frac{I_{DAi}(\Delta t_{i1})}{I_D^0 \alpha_{Di}} = 1 - \varepsilon_1, \tag{A1}$$

in which ε_1 was a small number of the order of 10^{-4}. Value of ε_1 should be small enough to ensure function $y_i(r, t)$ in Eq. 7 to remain practically equal to 1 for all distances r and for times belonging to the interval $(0, \Delta t_{i1})$. Under these conditions Eqs. A1 and 4 to 7 yield

$$\Delta t_{i1} = \frac{\varepsilon_1 \tau_{Di}}{1 + C_A^0 \dfrac{\pi R_0^6}{2 r_{min}^4}} \tag{A2}$$

The algorithm described in Kusba and Lakowicz (1994) allows to find the optimal length of the next step on the time axis based on the properties of the fluorescence decay in the previous time step, so knowing Δt_{i1} we were able to calculate Δt_{i2}, knowing Δt_{i2} we were able to calculate Δt_{i3}, and so on. In fact, this procedure allowed us to find times t_{ik} at which the intensity decays of the particular components had to be calculated. To calculate the decay function Eq. 5 for a given time t_{ik} one has to solve the diffusion Eq. 8. We applied here the procedure similar to that described in Kusba (1987). Eqs. 6 to 8 and the boundary conditions 10 and 11 were transformed to the Laplace space yielding

$$W_i(p) = \frac{k_i(p)}{p} = \frac{2\pi}{p^2} \int_{r_{min}}^{\infty} r k_{DAi}(r) z_i(r, p) dr \tag{A3}$$

$$\frac{d^2 z_i(r, p)}{dr^2} + \frac{1}{r}\frac{dz_i(r, p)}{dr} - \frac{1}{D}[p + k_{DAi}(r)] z_i(r, p) = -\frac{p}{D} \tag{A4}$$

$$\left[\frac{\partial z_i(r, p)}{\partial r}\right]_{r=r_{min}} = 0 \tag{A5}$$

$$z_i(r \to \infty, p) = 1 \tag{A6}$$

in which $z_i(r, p) = p y_i(r, p)$. The main stage of the procedure was the numerical solution of the linear differential Eq. A4 for the certain number of values of the parameter p. After that the appropriate integrals $W_i(p)$ were calculated and finally, using the Stehfest procedure (Stehfest, 1970) the $W_i(t_k)$ value was calculated by the numerical inversion of variables $W_i(p)$ to the time space.

We developed two different algorithms to solve the differential Eq. A4. According to our first algorithm, Eq. A4 was solved immediately, using the relaxation method. For a given set of parameters (p, D, τ_{Di}, R_0, and r_{min}) the solution included values of the function $z_i(r_j, p)$ calculated at 200 points r_j equally spaced in the interval $(r_{min}, r_{i\varepsilon})$. Because even an asymptotic solution of Eq. A4 is not known, the value of $r_{i\varepsilon}$, the upper limit of the interval, was calculated on the way different from that described in Kusba (1987). This quantity was estimated every time as that value of $r_{i\varepsilon}$, which with a good approximation fulfilled the condition

$$\left[\frac{dz_i(r, p)}{dr}\right]_{r=r_{i\varepsilon}} = \varepsilon_2, \tag{A7}$$

in which ε_2 was a small number of the order of 10^{-4}. Expression A7 may be understood as a consequence of the boundary condition A6. Such procedure allowed us to minimize the length of the calculation interval on the r axis and simultaneously to take the boundary condition A6 into account. It was assumed in further calculations that for $r > r_{i\varepsilon}$ the functions $z_i(r, p)$ are independent of r and equal to 1. After that, the quantities $W_i(p)$ were calculated using the relation

$$W_i(p) = \frac{2\pi}{p^2}\left[\int_{r_{min}}^{r_{i\varepsilon}} r k_{DAi}(r) z_i(r, p) dr + \int_{r_{i\varepsilon}}^{\infty} r k_{DAi}(r) dr\right]. \tag{A8}$$

First integral in Eq. A8 was calculated numerically based on the numerical solution of Eq. A4, whereas to evaluate the second integral an analytical expression was used.

According to the second algorithm, Eqs. A3 through A6 were transformed using the substitution

$$x = r^{-w} \tag{A9}$$

in which w is a positive real number. The main advantage of the transformation A9 is that using the equally spaced meshes on the x axis one obtains on the r axis smaller meshes for smaller values of r where the function $z_i(r, p)$ may dramatically increase with distance and larger meshes for higher values of r where function $z_i(r, p)$ practically remains equal to unity. This leads to more precise evaluation of the function $z_i(r, p)$ for smaller values of r where the transfer rate $k_{DAi}(r)$ in the first integral in Eq. A8 is large. Applying transformation A9 to Eqs. A4 to A6 one obtains

$$\frac{d^2 z_i(x, p)}{dx^2} + \frac{1}{x}\frac{dz_i(x, p)}{dx} - \frac{1}{Dw^2 x^s}[p + k_{DAi}(r)] z_i(x, p) = -\frac{p}{Dw^2 x^s} \tag{A10}$$

$$z_i(x = x_{min}, p) = 1 \tag{A11}$$

$$\left[\frac{dz_i(x, p)}{dx}\right]_{x=x_{max}} = 0 \tag{A12}$$

in which $s = 2(w + 1)/w$, $x_{imin} = r_{i\varepsilon}^{-w}$ and $x_{max} = r_{min}^{-w}$. Here $r_{i\varepsilon}$ was calculated from the formula

$$r_{i\varepsilon} = r_{min} + R_0[t_{ik}/(\varepsilon_3 \tau_{Di}]^{1/6} + 7\sqrt{D t_{ik}} \tag{A13}$$

with ε_3 being a small number of the order 10^{-6}. The aim of the formula (A13) is to evaluate a finite value of $r_{i\varepsilon}$ belonging to the interval (r_{min}, ∞) and simultaneously having the property that for $r \geq r_{i\varepsilon}$ functions $z_i(r, p)$ are with a good approximation equal to unity. The second term on the right side of Eq. A13 is the consequence of a condition that in the absence of diffusion $z_i(r \geq r_{i\varepsilon}, p) \geq 1 - \varepsilon_3$ and the third term takes into account possible diffusive modifications of the $z_i(r, p)$. Similarly as in our first algorithm, Eq. A10 was solved using the relaxation method. For a given set of parameters (p, D, $\tau_{Di}R_0$, and r_{min}) the solution of the equation consisted of 200 values of the function $z_i(x_k, p)$ calculated at 200 points x_k equally spaced in the interval (x_{imin}, x_{max}). After that, the quantities $W_i(p)$ were calculated using the relation

$$W_i(p) = \frac{2\pi}{p^2}\left[\frac{1}{w}\int_{x_{imin}}^{x_{max}} x^{-\frac{w+2}{w}} k_{DAi}(x) z_i(x, p) dx + \int_{r_{i\varepsilon}}^{\infty} r k_{DAi}(r) dr\right], \tag{A14}$$

which can be easily obtained from Eqs. A8 and A9. It appeared during the testing calculations that the optimum value of the parameter w is ~0.5, and this value was used in our analyses.

The application of the two algorithms in the data analysis programs showed that both of them recovered practically the same parameter values from our experimental data. However, by comparison of the results obtained with the diffusion coefficient set very small ($D \approx 10^{-15}$ cm^2/s) with the results given by analogous nondiffusive program we found out that the second algorithm is generally more precise. Besides, in all calculations the second algorithm appeared approximately four times faster than the first one. Certain disadvantage of the second algorithm is that because of using transformation A9 the value of r_{min} in this algorithm cannot be set too small. Here again the comparison of the results obtained from the diffusive program for $D \rightarrow 0$ with the results given by its nondiffusive analogue showed that the second algorithm provides satisfactorily precise calculations for $r_{mi} \geq 1$ Å.

This work was supported by grants from the National Institutes of Health, GM-35154 and RR-08119.

REFERENCES

Castellano, F. N., J. D. Dattelbaum, and J. R. Lakowicz. 1998. Long-lifetime Ru(II) complexes as labeling reagents for sulfhydryl groups. *Anal. Biochem.* 255:165–170.

Chen, J., and P. R. Selvin. 2000. Lifetime-and color tailored fluorophores in the micro- to millisecond time regime. *J. Am. Chem. Soc.* 122: 657–660.

Cheung, H. C. 1991. Resonance energy transfer. *In* Topics in Fluorescence Spectroscopy, Vol 2, Principles. J. R. Lakowicz, editor. Plenum Press, New York. 127–175.

Demas, J. N., and B. A. DeGraff. 1997. Applications of luminescent transition metal complexes to sensor technology and molecular probes. *J. Chem. Educ.* 74:690–695.

Dewey, T. G., and G. G. Hammes. 1986. Calculation of fluorescence resonance energy transfer on surfaces. *Biophys. J.* 32:1023–1036.

Edidin, M., M. C. Zuniga, and J. P. Sheetz. 1994. Truncation mutants define and locate cytoplasmic barriers to lateral mobility of membrane glycoproteins. *Proc. Natl. Acad. Sci. U.S.A.* 91:3378–3382.

Estep, T. N., and T. E. Thompson. 1979. Energy transfer in lipid bilayers. *Biophys. J.* 26:195–208.

Fulbright, R. M., D. Axelrod, W. R. Dunham, and C. L. Marcelo. 1997. Fatty acid alteration and the lateral diffusion of lipids in the plasma membrane of keratinocytes. *Exp. Cell Res.* 233:128–134.

Fung, B., and L. Stryer. 1978. Surface density measurements in membranes by fluorescence resonance energy transfer. *Biochemistry.* 17:5241–5248.

Gheber, L. A., and M. Edidin. 1999. A model for membrane patchiness: lateral diffusion in the presence of barriers and vesicle traffic. *Biophys. J.* 77:3163–3175.

Gryczynski, I., J. Kuśba, and J. R. Lakowicz. 1997. Effects of light quenching on the emission spectra and intensity decays of fluorophore mixtures. *J. Fluoresc.* 7:167–183.

Guo, X., L. Li, F. N. Castellano, H. Szmacinski, and J. R. Lakowicz. 1997. A long-lived, high luminescent rhenium (I) metal-ligand complex as a bimolecular probe. *Anal. Biochem.* 254:179–186.

Hauser, M., U. K. A. Klein, and U. Gösele. 1976. Extension of Förster's theory for long range energy transfer to donor-acceptor pairs in systems of molecular dimensions. *Z. Phys. Chem.* 101:255–266.

Horrocks, W. DeW., and D. R. Sudnick. 1981. Lanthanide ion luminescence probes of the structure of biological macromolecules. *Acc. Chem. Res.* 14:384–392.

Johnson, M. L. 1983. Evaluation and propagation of confidence intervals in nonlinear, asymmetrical variance spaces: analysis of ligand binding data. *Biophys. J.* 44:101–106.

Johnson, M. L., and S. G. Frasier. 1985. Nonlinear least squares analysis. *Methods Enzymol.* 117:301–342.

Jorgensen, K., A. Klinger, M. Brainman, and R. L. Biltonen. 1996. Slow nonequilibrium dynamical rearrangement of the lateral structure of a lipid membrane. *J. Phys. Chem.* 100:2766–1769.

Juris, A., V. Balzani, F. Barigelletti, S. Campagna, P. Belser, and A. Von Zelewsky. 1988. Ru(II)polypyridine complexes: photophysics, photochemistry, electrochemistry and chemiluminescence. *Coord. Chem. Rev.* 84:85–277.

Kalayanasundaram, K. 1992. *Photochemistry of Polypyridine and Porphyrin Complexes.* Academic Press, New York. 626.

Kenworthy, A. K., and M. Edidin. 1998. Distribution of a glycosylphosphatidylinositol-anchored protein at the apical surface of MDCK cells examined at a resolution of <100 Å using imaging fluorescence resonance energy transfer. *J. Cell Biol.* 142:69–84.

Kuśba, J. 1987. Long-range energy transfer in the case of material diffusion. *J. Luminesc.* 37:287–291.

Kuśba, J., and J. R. Lakowicz. 1994. Diffusion-modulated energy transfer and quenching: analysis by numerical integration of diffusion equation in laplace space. *Methods Enzymol. Num. Comp. Methods Part B.* 240:216–262.

Kuśba, J., G. Piszczek, I. Gryczynski, M. L. Johnson, and J. R. Lakowicz. 2000. Effects of diffusion on energy transfer in solution using a microsecond decay time rhenium metal-ligand complex as the donor. *Chem. Phys. Letts.* 319:661–668.

Lakowicz, J. R. 1999. *Principles of Fluorescence Spectroscopy*, 2nd Edition. Kluwer Academic/Plenum Publishers, New York. 698. In this reference eq. 15.22 on page 437 should contain the term τ_D in the denominator of the right-most term.

Lakowicz, J. R., and I. Gryczynski. 1991. Frequency-domain fluorescence spectroscopy. *In* Topics in Fluorescence Spectroscopy, Vol. 1: Techniques. J. R. Lakowicz, editor. Plenum Press, New York. 293–337.

Lakowicz, J. R., G. Piszczek, and J. S. Kang. 2001. On the possibility of long-wavelength long-lifetime high-quantum yield luminophores. *Anal. Biochem.* 288:62–75.

Li, L., F. N. Castellano, I. Gryczynski, and J. R. Lakowicz. 1999a. Long-lifetime lipid rhenium metal-ligand complex for probing membrane dynamics on the microsecond timescale. *Chem. Phys. Lipids.* 99:1–9.

Li, L., I. Gryczynski, and J. R. Lakowicz. 1999b. Resonance energy transfer study using a rhenium metal-ligand lipid conjugate as the donor in a model membrane. *Chem. Phys. Lipids.* 101:243–253.

Li, L., H. Szmacinski, and J. R. Lakowicz. 1997. Synthesis and luminescence spectral characterization of long-lifetime lipid metal-ligand probes. *Anal. Biochem.* 244:80–85.

Li, M., and P. R. Selvin. 1995. Luminescent polyaminocarboxylate chelates of terbium and europium: the effect of chelate structure. *J. Am. Chem. Soc.* 117:8132–8138.

Lippincott-Schwartz, J., J. F. Presley, K. J. M. Zaal, K. Hirschberg, C. D. Miller, and J. Ellenberg. 1999. Monitoring the dynamics and mobility of membrane proteins tagged with green fluorescent protein. *Methods Cell Biol.* 58:261–281.

Maliwal, B. P., Z. Gryczynski, and J. R. Lakowicz. 2001. Long-wavelength long-lifetime luminophores. *Anal. Chem.* 73:4277–4285.

Marguet, D., E. T. Spiliotis, T. Pentcheva, M. Lebowitz, J. Schneck, and M. Edidin. 1999. Lateral diffusion of GFP-tagged H2L^d molecules and of GFP-TAP1 reports on the assembly and retention of these molecules in the endoplasmic reticulum. *Immunity.* 11:231–240.

Marra, J. 1986. Direct measurement of the interaction between phosphatidylglycerol bilayers in aqueous electrolyte solutions. *Biophys. J.* 50: 815–825.

Martin, R. B., and F. S. Richardson. 1979. Lanthanides as probes for calcium in biological systems. *Q. Rev. Biophys.* 12:181–209.

Matko, J., and M. Edidin. 1997. Energy transfer methods for detecting molecular clusters on cell surfaces. *Methods Enzymol.* 278:444–462.

Periasamy, N., and A. S. Verkman. 1998. Analysis of fluorophore diffusion by continuous distributions of diffusion coefficients: application to pho-

tobleaching measurements of multicomponent and anomalous diffusion. *Biophys. J.* 75:557–567.

Sabbatini, N., and M. Guardigli. 1993. Luminescent lanthanide complexes as photochemical supramolecular devices. *Coord. Chem. Rev.* 123: 201–228.

Simson, R., E. D. Sheets, and K. Jacobson. 1995. Detection of temporary lateral confinement of membrane proteins using single-particle tracking analysis. *Biophys. J.* 69:989–993.

Stehfest, H. 1970. Algorithm 368: numerical inversion of laplace transforms. *Commun. ACM* 13:47–49.

Stehfest, H. 1970. Remark on algorithm 368: numerical inversion of laplace transforms. 13:624.

Steinberg, I. Z., and E. Katchalski. 1968. Theoretical analysis of the role of diffusion in chemical reactions, fluorescence quenching, and nonradiative energy transfer. *J. Chem. Phys.* 48:2404–2410.

Struck, D. K., and R. E. Pagano. 1980. Insertion of fluorescent phospholipids into the plasma membrane of a mammalian cell. *J. Biol. Chem.* 255:5404–5410.

Stryer, L., D. D. Thomas, and C. F. Meares. 1982. Diffusion enhanced fluorescence energy transfer. *Ann. Rev. Biophys. Bioeng.* 11:203–222.

Stubbs, C. D., and B. W. Williams. 1992. Fluorescence in membranes. *In* Topics in Fluorescence Spectroscopy, Vol 3, Biochemical Applications. J. R. Lakowicz, editor. Plenum Press, New York. 231–271.

Szmacinski, H., E. Terpetschnig, and J. R. Lakowicz. 1996. Synthesis and evaluation of Ru-complexes as anisotropy probes for protein hydrodynamics and immunoassays of high-molecular-weight antigens. *Biophys. Chem.* 62:109–120.

Tanhuanpää, K., and P. Somerharju. 1999. γ-Cyclodextrins greatly enhance translocation of hydrophobic fluorescent phospholipids from vesicles to cells in culture. *J. Biol. Chem.* 274:35359–35366.

Terpetschnig, E., J. D. Dattelbaum, H. Szmacinski, and J. R. Lakowicz. 1997. Synthesis and spectral characterization of a thiol-reactive long-lifetime Ru(II) complex. *Anal. Biochem.* 251:241–245.

Terpetschnig, E., H. Szmacinski, H. Malak, and J. R. Lakowicz. 1995. Metal-ligand complexes as a new class of long-lived fluorophores for protein hydrodynamics. *Biophys. J.* 68:342–350.

Thomas, D. D., W. F. Caslsen, and L. Stryer. 1978. Fluorescence energy transfer in the rapid diffusion limit. *Proc. Natl. Acad. Sci. U.S.A.* 75:5746–5750.

Thomas, D. D., and L. Stryer. 1982. Transverse location of the retinal chromophore of rhodopsin in rod outer segment disc membranes. *J. Mol. Biol.* 154:145–157.

Thompson, T. E., M. B. Sankaram, R. L. Biltonen, D. Marsh, and W. L. C. Vaz. 1995. Effects of domain structure on in-plane reactions and interactions. *Mol. Membr. Biol.* 12:157–162.

Tocanne, J.-F., L. Dupou-Cezanne, and A. Lopez. 1994. Lateral diffusion of lipids in model and natural membranes. *Prog. Lipid Res.* 33:203–237.

Tyson, D. S., and F. N. Castellano. 1999. Light-harvesting arrays with coumarin donors and MLCT acceptors. *Inorg. Chem.* 38:4382–4383.

Tyson, D. S., and F. N. Castellano. Intramolecular singlet and triplet energy transfer in a ruthenium(II) diimine complex containing multiple pyrenyl chromophores. *J. Phys. Chem. A.* 103:10955–10960.

Velez, M., and D. Axelrod. 1988. Polarized fluorescence photobleaching recovery for measuring rotational diffusion in solutions and membranes. *Biophys. J.* 53:575–591.

Walther, D., P. Kuzmin, and E. Donath. 1996. Brownian dynamics simulation of the lateral distribution of charged membrane components. *Eur. Biophys. J.* 24:125–135.

Wolber, P. K., and B. S. Hudson. 1979. An analytic solution to the problem of Förster energy transfer problem in two dimension. *Biophys. J.* 28: 197–210.

Zhang, F., G. M. Lee, and K. Jacobson. 1993. Protein lateral mobility as a reflection of membrane microstructure. *BioEssays* 15:579–588.

Zhou, X., D. S. Tyson, and F. N. Castellano. 2000. First generation light-harvesting dendrimers with a $[Ru(bpy)_3]^{2+}$ core and aryl ether ligands functionalized with coumarin 450. *Angew. Chem. Int. Ed.* 39: 4301–4305.

Zucker, S. D. 2001. Kinetic model of protein-mediated ligand transport: influence of soluble binding proteins on the intermembrane diffusion of a fluorescent fatty acid. *Biochemistry*. 40:977–986.